Computers and Chemical Engineering 49 (2013) 1–17

Contents lists available at SciVerse ScienceDirect

Computers and Chemical Engineering

journal homepage: www.elsevier.com/locate/compchemeng

Experimental and computational modeling of oscillatory flow within a baffled tube containing periodic-tri-orifice baffle geometries

Xesús Nogueira[a,*], Benjamin J. Taylor[b], Hector Gomez[a], Ignasi Colominas[a], Malcolm R. Mackley[b]

[a] Group of Numerical Methods in Engineering, Dept. of Applied Mathematics, Universidade da Coruña, Campus de Elviña, 15071 A Coruña, Spain
[b] Department of Chemical Engineering and Biotechnology, University of Cambridge, New Museums Site, Pembroke Street, Cambridge CB23RA, UK

ARTICLE INFO

Article history:
Received 26 March 2012
Received in revised form
19 September 2012
Accepted 21 September 2012
Available online 16 October 2012

Keywords:
Oscillatory flow mixing
Simulation
CFD
Fluid mechanics
Turbulence
Visualization

ABSTRACT

This paper describes numerical simulation and matching experimental results for oscillatory flow within a baffled tube containing tri-orifice baffles. The numerical simulation implemented a non-standard approach based on Implicit Large Eddy Simulation (ILES) to predict the flow in a situation where complex eddy formation occurs due to periodic separation for each oscillation of the flow. The set of performed experiments showed that within the cavity between each baffle, the flow structure was complex with elements of periodicity and a wide range of length scales. Conventional Large Eddy Simulation and comparison with experiments were used to validate the ILES results. It was concluded that the gross flow structure was captured by ILES, indicating that the numerical scheme is suitable for computation in the complex flow situation. In addition, ILES methodology was used to study the effect of increasing the oscillation frequency on the radial and axial velocities.

1. Introduction

Oscillatory flow mixing (OFM) occurs when fluid is oscillated via bellows, diaphragm or piston action through a series of baffled constrictions, and the base mixing mechanism is achieved by the generation of successive vortex rings as the flow passes through each of the baffle constrictions (Mackley & Ni, 1991). The eddy mixing produced by the periodic flow is sufficient to result in radial velocity components having similar magnitudes to the axial velocity components, thereby producing a situation where each cavity region between successive baffles acts in a similar way to a well-mixed stirred tank (Harvey, Mackley, & Stonestreet, 2001; Palma & Giudici, 2003). OFM finds a broad number of industrial applications, including wastewater treatment, biofuels and fine chemicals production, and bioprocessing, with outstanding improvements in selectivity and quality for productions in the range of kilograms-per-day up to tonnes/hour (Smith & Mackley, 2001).

Fig. 1 schematically shows the basic mechanism of OFM in a horizontal single-orifice baffled tube. As the fluid passes through the constrictions, vortex rings form downstream of each baffle orifice (A) and translate axially (B) in the direction of applied flow until the applied flow direction changes (C) and then vortices in the opposing directions collide (D). The amplitude and frequency of oscillation control the mixing and are independent mixing parameters. The governing dimensionless groups for OFM are Mackley, Smith, and Wise (1993):

$$Re_o = \frac{2\pi f x_0 \rho d_e}{\mu} \quad (1)$$

$$St = \frac{d_e}{4\pi x_0} \quad (2)$$

where Re_o is the oscillatory Reynolds number, ρ is the fluid density, μ is the fluid viscosity, f is the frequency of oscillation, x_0 is the centre-to-peak amplitude of oscillation, St is the Strouhal number and d_e is the effective tube diameter defined as Smith (1999):

$$d_e = \sqrt{\frac{d^2}{n}} \quad (3)$$

where d is the tube diameter and n is the number of orifices in the baffle.

Re_o describes the mixing intensity caused by $2\pi f x_0$, the maximum oscillatory velocity, and St is the ratio of the tube diameter to the amplitude of oscillation. The inter-baffle spacing is of importance to achieve good mixing within oscillatory flow and is based on d_e of the tube such that baffle spacing is equal to 1.5 d_e. In Smith (1999) it was shown that the flow patterns of OFM using n-hole multi-hole baffle configurations were similar to those generated with a single-orifice baffle configuration in terms of eddy formation

* Corresponding author. Tel.: +34 981 167 000; fax: +34 981 167 170.
E-mail address: xnogueira@udc.es (X. Nogueira).

0098-1354/$ – see front matter © 2012 Elsevier Ltd. All rights reserved.
http://dx.doi.org/10.1016/j.compchemeng.2012.09.015

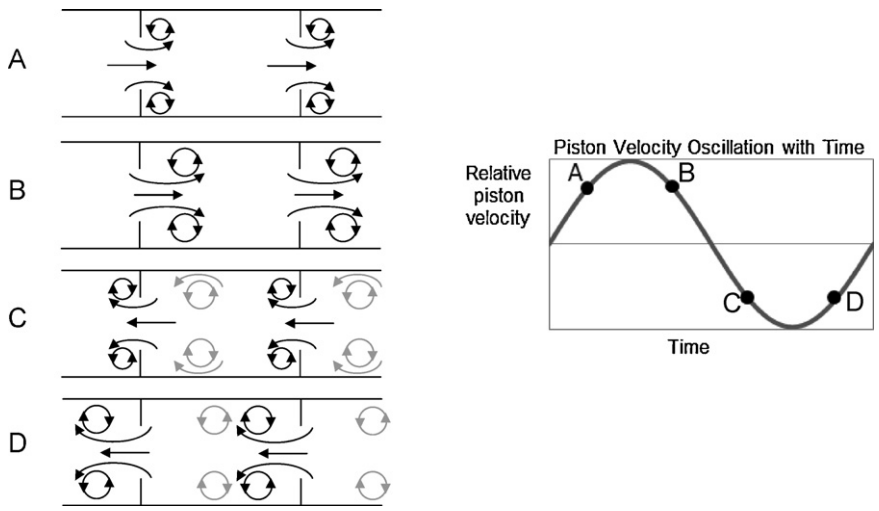

Fig. 1. Mechanism of OFM in a single-orifice baffled tube (see Fitch, Jian, & Ni, 2005), demonstrated by four points throughout an oscillation cycle.

and propagation from individual orifices. However, slight deviations between the flow resulting from the two different geometries were likely due to interaction between eddies generated from adjacent orifices of the same baffle in the multi-hole configuration. The multi-hole baffle configurations were presented as advantageous to scale-up in larger diameter tubes because the same shear rates and intensity of mixing could be expected in a larger volume tube with multi-hole baffles as would be experimentally determined at much smaller laboratory and pilot scales with either multi-orifice or single-orifice baffle configurations. Large tubes with single-hole baffles, on the other hand, were scalable but did not exhibit the same level of flow similarity upon scale-up from small tubes. This is an important consideration for real-world engineering applications, and as such the current work explores the flow of a common Newtonian fluid (water) in this scalable tube geometry. In this paper a tri-orifice baffle ($n = 3$) was chosen as it was considered to give efficient mixing for the tube diameter of 60 mm used in the experimental work.

Fluid oscillation within this type of geometry is capable of generating complex eddy structures, and the flow exhibits eddies whose characteristic length scales vary over several orders of magnitude. The larger eddies are mainly dependent upon the geometry and boundary conditions, while the smaller are universal for complex flow dissipative systems (Wilcox, 1994). Direct simulation of turbulent flows requires extremely fine computational grids to resolve all the features of the flow. In practical application, this is unattainable, therefore most calculations need to be performed on meshes that do not have enough resolution to capture the smaller eddies of the flow. The use of computational meshes which lack the necessary spatial resolution may cause instabilities in the calculations, leading to unacceptable solutions (Nogueira, Cueto-Felgueroso, Colominas, & Khelladi, 2010). Traditionally, this problem has been dealt with by modeling turbulence rather than directly solving the fundamental equations of fluid mechanics. The approximation models of turbulence may be performed in several ways, but almost invariably lead to modification of the Navier–Stokes equations with new terms, which are not known *a priori*. Here it is argued that an adequate numerical discretization of the Navier–Stokes equations may play the role of a turbulence approximation model in a similar manner to a filter-based Large Eddy Simulation (LES), while avoiding the use of *ad hoc* parameters, such as the so-called eddy viscosity, nor requiring additional subgrid scale (SGS) models. The numerical discretization technique used in this paper will be referred to as Implicit Large Eddy Simulation (ILES) and is based on the idea of Monotonically Integrated Large-Eddy Simulation (MILES) for the computation of turbulent flows. This approach has been used in Boris, Grinstein, Oran, and Kolbe (1992), Oran and Boris (1993), Porter, Pouquet, and Woodward (1994), Margolin, Smolarkiewicz, and Sorbjan (1999), Grinstein and Fureby (2002), and Margolin and Rider (2002) to compute high Reynolds bounded flows and supersonic flows among others. Note that in this approach no "turbulence model" is used. This is explained in Section 3.

Previous simulations of oscillatory fluid flow in an oscillatory baffled column with single orifice baffle geometry employed the use of Reynolds-averaged Navier–Stokes (RANS) or LES turbulence models (Jian & Ni, 2003; Ni, Jian, & Fitch, 2002, 2003). These models have also been used for the simulations of other mixing devices (Coroneo, Montante, Paglianti, & Magelli, 2011; Jaworsky & Dudczak, 1998). Here, we propose the use of an ILES methodology for the computation of a three-orifice oscillatory-baffled tube (OBT), using FLUENT. To the best of our knowledge, this is the first time that an OBT with such a complex geometry has been simulated. The ILES technique renders a simple and effective methodology, since neither a SGS model nor additional ad-hoc parameters are required, in contrast to previous approaches such as RANS or conventional LES. The computational approach presented here is consistent meaning that the solution converges to the Direct Numerical Simulation (DNS) as the grid is refined (that is, it converges to the solution obtained by solving the Navier–Stokes equations). Note that this is not the case in other approaches using the eddy-viscosity concept. The effectiveness of ILES is demonstrated by applying it to the prediction of flow patterns and axial and radial velocities at some interrogation areas for two different flow regimes. ILES results are compared with experimental images and also with the simulations using a more usual approach for LES [Smagorinsky–Lilly model (Smagorinsky, 1963) and Dynamic-Smagorinsky model (Germano, Piomelli, Moin, & Cabot, 1991)].

The results show that the use of ILES in the context of oscillatory baffled tubes is a feasible methodology to obtain numerical results that accurately match with the experimental results. In summary, the approach described here can be considered a simple and effective predictive tool for the computation of flow patterns in oscillatory baffled tubes.

Following a demonstration of the suitability of the ILES methodology for the simulation of oscillatory flow mixing within the tube, ILES is used to study the effect of the oscillation frequency on the mixing capabilities of the OBT. Axial and radial velocities are used to describe this feature of the device.

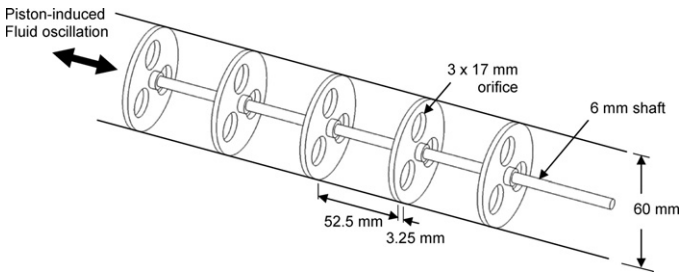

Fig. 2. Schematic showing a series of segments within an oscillatory baffled tube.

The paper is organized as follows. In Section 2, the experimental setup and procedure used to obtain the experimental images are described. In Section 3, ILES is described, after a brief discussion about the idea of Large Eddy Simulation and some considerations about dispersion and dissipation numerical errors. Then, Section 4 is devoted to ILES and LES numerical simulations and the comparison with experimental results, to validate the use of ILES methodology. After validation, ILES is used to study the effect of oscillation frequency on the flow features. Finally, the conclusions are drawn in Section 5.

2. Apparatus and experimental methods

A horizontal 1-l batch oscillatory baffled tube was constructed of Perspex with a stainless steel shaft and baffles. A linear actuator powered a piston that oscillated the fluid contents of the tube. A schematic of the experimental and simulation geometry boundary conditions used in this paper is shown in Fig. 2. Both baffle spacing of 52.5 mm and baffle constriction ratio (fraction of solid baffle area to tube cross-sectional area) of 0.76 were established from experience of the authors with single- and multi-orifice geometries previously tested.

Fig. 3(a) shows a schematic of the components utilized for the visualization experiments, and Fig. 3(b) shows a side elevation schematic of the light path through the tube. Highly reflective polyamide particles of 20 μm ($RD = 1.02$) were used as passive, solid tracers in reverse osmosis water, and a small addition of washing-up liquid acted as a dispersant. A section of the Perspex tube was encapsulated in a viewing box filled with glycerol to correct for the refractive index. The entire setup was shielded from interference of ambient light, and a mercury lamp (mains supply of 230 V at 50 Hz) provided focused, high-intensity illumination necessary for the experiments. A mirror directed the beam of light through a slit oriented so as to create a thin plane of light spanning one middle segment of the tube (bounded either side by baffles). A high-speed, high-resolution camera positioned perpendicularly to the thin plane of light then captured the light reflected off the suspended tracer particles within the plane. The camera shutter speeds were 1/500 and 1/1000 with frame rates of 500 and 1000 fps, respectively. The shutter speeds were chosen to obtain the clearest images of the particles in motion for the Re_o evaluated.

For flow visualization, sequential frames were added using code written in MATLAB, such that each pixel's greyscale value was

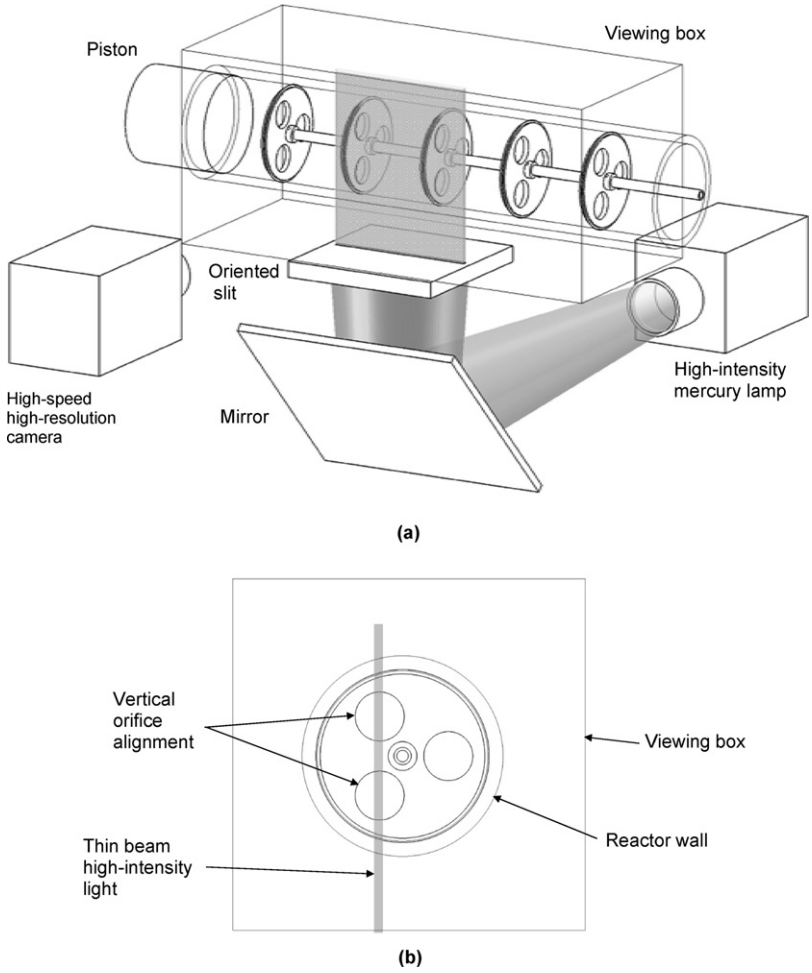

Fig. 3. Experimental setup schematics for flow visualization. Perspective view (a) and side elevation (b). In (b) the interrogation plane is shaded in grey.

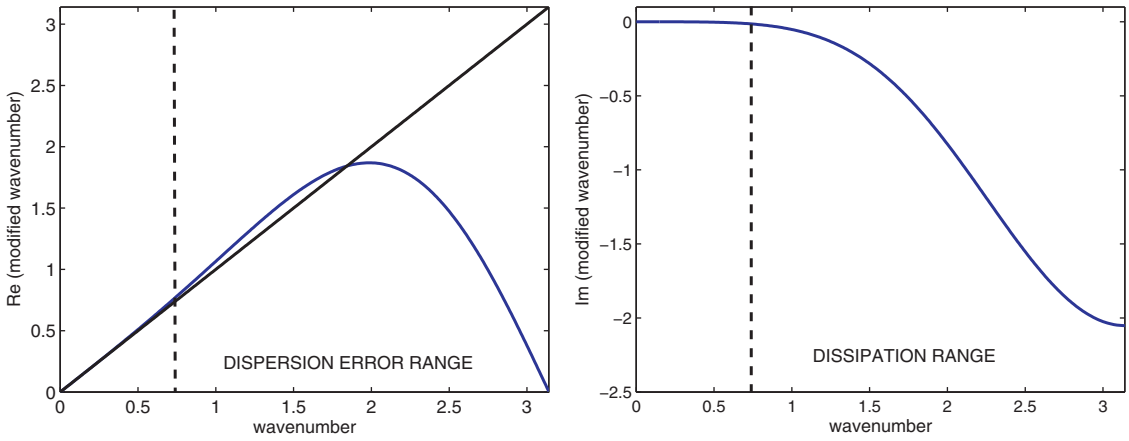

Fig. 4. Dispersion and dissipation curves of an third-order upwind numerical scheme for the advection equation (see Nogueira, Cueto-Felgueroso, Colominas, & Gómez, 2010). It is observed the wavenumber range of dispersion error that matches the dissipation range.

determined and compared with the value for the same pixel location in the previous frame. The highest greyscale value achieved for each pixel was saved and combined with the other pixels' highest values to generate an image very similar to one created using a long exposure time. This method allowed precise control for creation of flow images of desired phase positions.

For PIV analysis, the raw photographs covering 10 oscillation cycles were first processed using URAPIV software. The open-source software worked by analyzing a stack of photographs, two at a time, such that the particles in suspension were identified by location and their displacements and trajectories tracked between the two sequential photographs. The software recorded the original position, the distance traveled in the x-direction and the distance traveled in the y-direction of the light plane. The interrogation area used was 64×64 pixels with a grid spacing of 8 pixels. These conditions were appropriate to consistently obtain accurate results across all experiments. Accuracy of the grid spacing and interrogation area was checked by comparing the results with other grid sizes and interrogation areas. The resulting data file from the URAPIV output was then processed using MATLAB code generated specifically for this study. The code was used to plot the data as vector fields across the entire inspection plane.

Laser Doppler Velocimetry (LDV) was used to validate PIV results as well as to study axial velocities near the baffle orifices. The experiments are described more in context in Section 4.1.3.

3. Computational modeling

Many of the numerical simulations in oscillatory flow mixing have been performed using LES. However, simulations have been published recently (Jian & Ni, 2005) where the so-called "laminar" solver is used instead of a LES approach, even though the conditions of the flow are similar to those simulated using LES. The use of "laminar" solver can be seen as an Implicit Large Eddy Simulation (ILES). In this section we justify this assertion.

As it is known, any turbulent flow presents a wide range of length scales, and these can be identified with eddies of different sizes in the flow (Pope, 2000). The most significant part of the kinetic energy of a turbulent flow is contained in larger eddies (or larger scales). These vortices are created by instabilities of the mean flow and they are also under the action of inertial instabilities that may break the large eddies down into smaller ones. The new smaller vortices are also under the action of instabilities and they may break again. Each time that a vortex breaks, its energy is transferred to the new smaller structures. This breaking-vortex event is continuously taking place in a flow and it is called the *energy cascade*. The cascade process is dominated by inertial forces and the viscosity does not take part in it (note that for a wall-bounded flow, this would not be true near the walls). However, from a certain size of the smaller scales, the Reynolds number based on the eddy length scale takes a value small enough to obtain stable eddy motion. At this moment, viscous forces are not negligible and dissipation becomes important, as the energy is not transferred but dissipated by viscous forces. The range of scales for which this happens is called the dissipation range. In this range, the smallest scale for what the Reynolds number based on the eddy length scale equals to 1 is called *Kolmogorov scale* (Kolmogorov, 1991).

3.1. Implicit Large-Eddy Simulation (ILES)

If a numerical simulation is not able to solve the whole range of scales, the energy cascade is truncated at some point. Thus, the smaller scales present in the grid have certain energy that is neither transferred nor dissipated. If the numerical scheme does not have a dissipative mechanism, the energy of these scales will increase and the simulation will crash. This phenomenon is usually referred to as energy pile-up (Davidson, 2010).

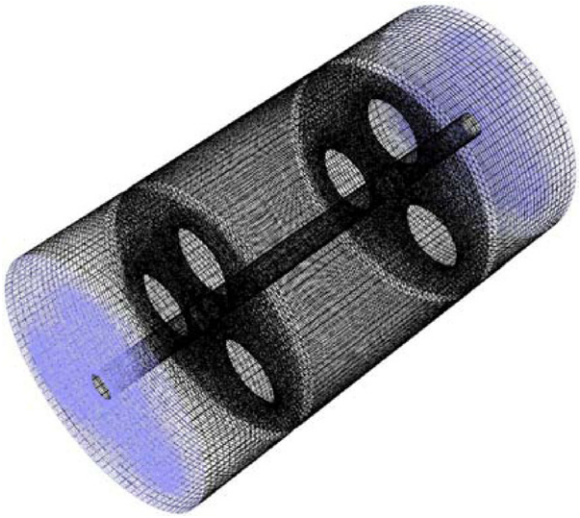

Fig. 5. Computational domain for the simulation of fluid flow in a three-orifice OBT. The computational mesh is composed of approximately 1 900 000 cells. Inlet boundaries are marked in blue.

Classical LES approaches use the filtered Navier–Stokes equations to remove the smaller eddies. As a consequence of filtering a set of unknown terms appear (Wilcox, 1994). These new terms correspond to eddies with sizes smaller than the filter size (*subgrid scale* terms) and they need to be modeled. One of the most popular approaches is the Smagorinsky–Lilly model (Lilly, 1966), a modification of the Smagorinsky model (Smagorinsky, 1963; Wilcox, 1994). The Smagorinsky–Lilly model is based on the idea of *eddy viscosity*. Most LES simulations of oscillatory flow mixing (OFM) have been done using Smagorinsky-based LES. However, it is known that this model is very dissipative. An improvement to the classical Smagorinsky model is the Dynamic model (Germano et al., 1991). In this model, the constant parameter of the Smagorinsky–Lilly model is dynamically computed at each time step.

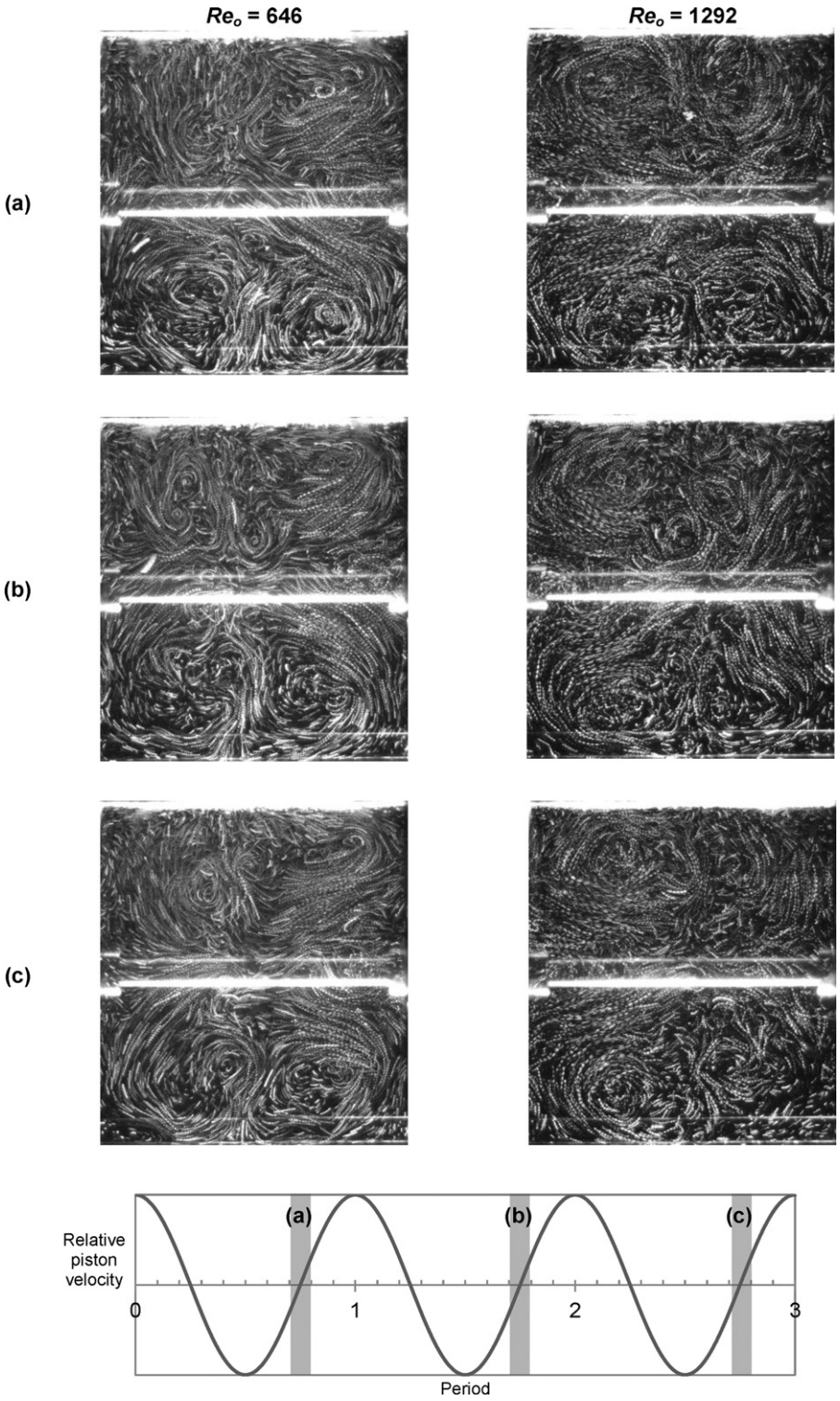

Fig. 6. Experimental flow visualization of the same phase position for successive piston oscillations for Re_o = 646 (f = 1 Hz) and Re_o = 1292 (f = 2 Hz) illustrating period repeating flow features dependent upon piston phase position (St = 1.0, x_0 = 2.65 mm). The images show the entire region between two baffles.

Most subgrid scale models are based on the eddy viscosity concept. The main assumption of these models is that the action of the subgrid scales on the resolved scales is purely dissipative. However, most numerical methods introduce some dissipation. The idea behind *Implicit Large-Eddy Simulation* (ILES) techniques is that this amount of *numerical* dissipation is enough to remove the high-scale energy, without explicit subgrid modeling.

In this paper we use a Monotone Upstream-Centered Scheme for Conservation Laws (MUSCL) numerical scheme based on a blending between a second-order upwind scheme and a central-differencing scheme (ANSYS, 2009) to compute ILES simulations, whereas LES simulations are computed using a second-order-accurate central differencing discretization with deferred approach (ANSYS, 2009). Upwind discretization is based on numerical differentiation biased in the direction determined by the sign of the characteristic speeds, and is widely used to solve the Navier–Stokes equations. This numerical discretization introduces some amount of numerical dissipation. Thus, the use of upwind methods for LES is controversial (Beaudan & Moin, 1994; Mittal & Moin, 1997), due to the excessive dissipation in coarse grids. On the other hand, the use of upwind methods for LES without any SGS model has been proposed in Boris et al. (1992), Oran and Boris (1993), Porter et al. (1994), Margolin et al. (1999), Grinstein and Fureby (2002), and Margolin and Rider (2002). This approach is known as the *Monotonically Integrated Large-Eddy Simulation* (MILES). In some of the MILES approaches, the physical viscosity is set to zero (Porter, Pouquet, & Woodward, 1992), and all the viscosity (also molecular viscosity) is introduced by the numerical method. The authors have shown that the amount of dissipation of upwind discretizations mainly depends on the quality of the approximation of the derivatives computed for the reconstruction step of the variables required in high-order upwind methods (Nogueira, Cueto-Felgueroso, Colominas, & Gómez, 2010).

More elaborate ways of computing the subgrid scales without the use of a turbulence model are presented in Codina, Principe, Guasch, and Badia (2007) and Bazilevs et al. (2007). In these approaches, the effect of the subgrid scales is not assumed to be strictly dissipative.

In the viscous layers close to the wall, it is the viscosity, and not the self-similar cascade, the predominant mechanism that drives the energy. The flow structures have a well-defined length scale there (Jiménez, 2007). In order to use ILES approach in wall-bounded flows, numerical techniques such as wall modeling could be used near walls if the boundary layer is not completely solved.

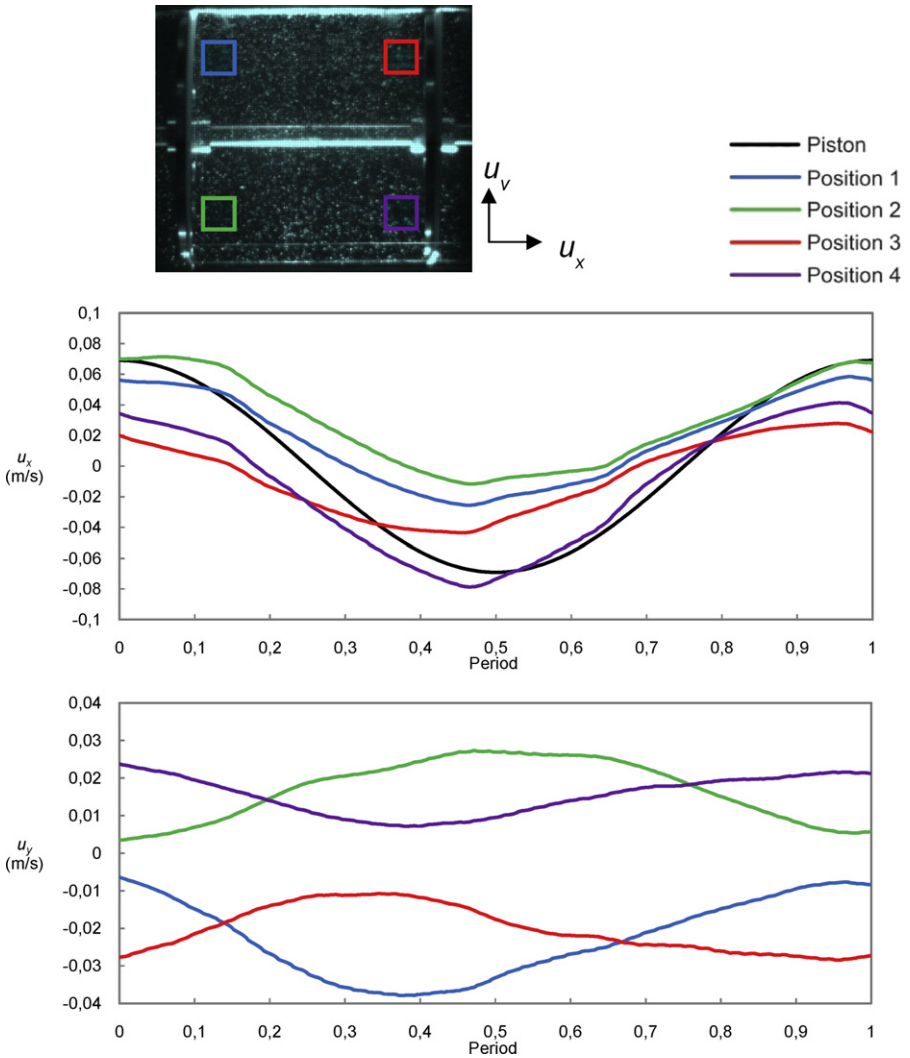

Fig. 7. Experimental phase-averaged local axial (u_x) and radial (u_y) velocities of selected regions within the OBT during piston oscillation ($Re_o = 646$, $St = 1.0$, $f = 1$ Hz, $x_0 = 2.65$ mm).

3.2. Dispersion and dissipation errors of a numerical scheme

In order to illustrate the approach used here, an explanation is given in terms of the dispersion and dissipation errors of a numerical scheme when the pure advection equation is solved. Even though this is a very simplified case, it helps to understand the effect of the numerical method on the solution.

The Fourier modes of exact solutions to the advection equation verify a relationship called dispersion relation that links its wavenumber κ with its frequency ω. For the one-dimensional advection equation with a constant velocity field a, the dispersion relation is simply $\omega = a\kappa$.

The discretization of the advection equation usually introduces both dispersion and dissipation errors. The dispersion error is related to the amount by which the numerical solution fails to satisfy the dispersion relation. The dissipation error is created by artificial diffusion introduced by the algorithm, which is not present in the exact solution (see Nogueira, Cueto-Felgueroso, Colominas, & Khelladi, 2010 and references therein for a more elaborated explanation). These errors could be expressed in terms of a *modified* wavenumber. If the wavenumber and the modified wavenumber are different, each Fourier component of the numerical wave will propagate with a different velocity than the real one. Moreover, if the modified wavenumber is complex, dissipation errors will appear (and the wave will be damped out as it propagates). This is common in many numerical methods, such as, for example, upwind methods. Fig. 4 shows a plot of the dissipation curve of a third-order upwind numerical scheme (Nogueira, Cueto-Felgueroso, Colominas, & Khelladi, 2010). The real wavenumber (horizontal axis) is plotted versus the real and the imaginary part of the modified wavenumber (vertical axis). When the imaginary part of the modified wavenumber is zero, there is no dissipation, just as in the exact solution to the pure advection equation. In the dispersion curve, the solid black line is the curve of an ideal

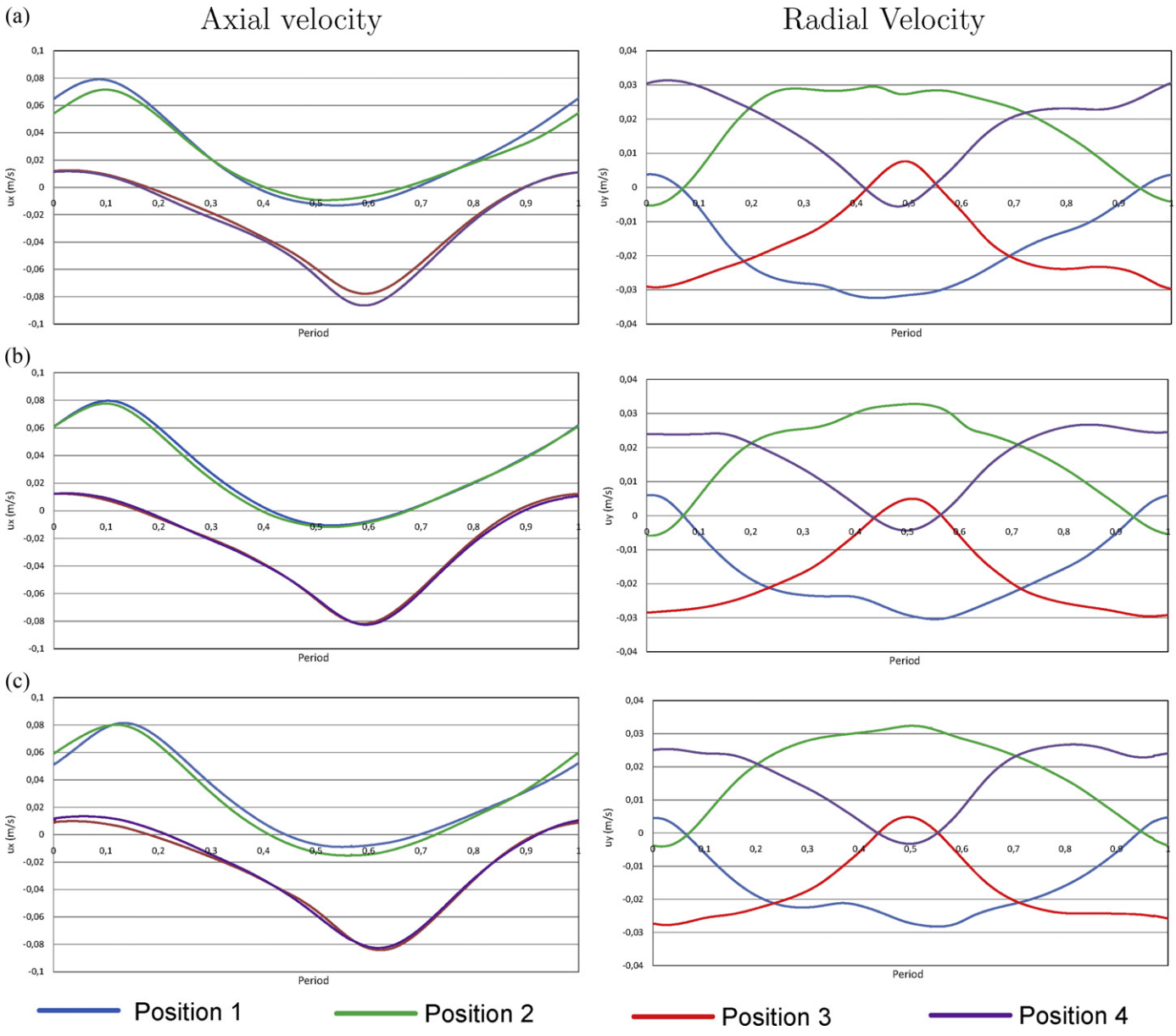

Fig. 8. Numerical results of phase-averaged local axial (left) and radial (right) velocities of selected regions within the OBT during piston oscillation ($Re_o = 646$, $St = 1.0$, $f = 1$ Hz, $x_0 = 2.65$ mm). (a) ILES, (b) Smagorinsky–Lilly LES, and (c) Dynamic-Smagorinsky LES results.

method without dispersion error, that is, the real part of the modified wavenumber matches the physical wavenumber. Moreover, it shows that the numerical scheme does not introduce dissipation for wavenumbers smaller than a cut-off value. It is also observed that numerical dissipation is introduced in the range of wavenumbers with larger dispersion error.

The ideas obtained from the study of the 1D advection equation can be extrapolated to some extent to the Navier–Stokes equations. Then, the proposed argument for the use of Implicit Large Eddy Simulation is as follows: It is assumed that the numerical scheme will accurately resolve the energy-containing range and the inertial subrange (in case the flow has a well-defined inertial subrange), but it will damp out the energy contained in the dissipation range, as illustrated in Fig. 4. Following Pope (2000), most of the scales are included in the dissipation range, and only a small part of them are included in the energy-containing range and inertial subrange. Thus, the larger eddies of the flow are accurately solved, and the smaller eddies are somehow modeled through the use of numerical damping in the dissipation range. It is proposed that this conceptualization follows the spirit of LES, and thus, is referred to as Implicit Large Eddy Simulation (ILES). Here ILES of a tri-orifice OBT using a third-order upwind scheme is presented, and it is argued to be a viable alternative to classical approaches, such as RANS or LES.

4. Numerical methods and simulations

Incompressibility was assumed throughout the fluid, and thus the three-dimensional Navier–Stokes equations were solved, namely,

$$\frac{\partial u_i}{\partial x_i} = 0$$
$$\frac{\partial u_i}{\partial t} + u_j \frac{\partial u_i}{\partial x_j} = \frac{\partial}{\partial x_j}\left(\nu \frac{\partial u_i}{\partial x_j}\right) - \frac{1}{\rho}\frac{\partial p}{\partial x_i} \quad (4)$$

In the set of Eq. (4), ρ is the density, p is the pressure, ν is the kinematic viscosity and $\boldsymbol{u} = (u_1, u_2, u_3)$ is the velocity vector. It is assumed that repeated indices indicate summation.

The system (4) was solved on the domain shown in Fig. 5. The computational domain spanned a baffled cell, and additionally, half of the following and previous baffled cells were included in order to correctly impose periodic boundary conditions. The mesh was unstructured and consisted of approximately 1 900 000 cells (see Fig. 5). FLUENT (ANSYS, 2009) was used to perform the simulations. As commented above, wall-boundary conditions for turbulent flows are a difficult issue. In a pure ILES framework, the boundary layer has to be solved directly. However, this is not practical since it requires a very fine grid. In this work, when the mesh is not fine enough to resolve the viscous sublayer a logarithmic expression is used to model the mean velocity (ANSYS, 2009).

Imposed inlet conditions were located at the inlet faces of the fixed grid (shown in blue in Fig. 5) and were defined using a User Defined Function (UDF) to impose the mass flow rate as a function of time:

$$\dot{m}(t) = \frac{1}{2}\rho\pi^2 d^2 f x_0 \cos(2\pi f t) \quad (5)$$

where d is the diameter of the tube, f is the frequency of oscillation of the piston, x_0 is the centre-to-peak amplitude of oscillation and t is the time. The fluid was defined by $\rho = 998.2\ \mathrm{kg/m^3}$ and $\mu = 0.00089$ Pa s.

Two flow conditions are presented, defined as follows:

(1) $Re_o = 646$, $St = 1.0$, $f = 1$ Hz, $x_0 = 2.65$ mm
(2) $Re_o = 1292$, $St = 1.0$, $f = 2$ Hz, $x_0 = 2.65$ mm

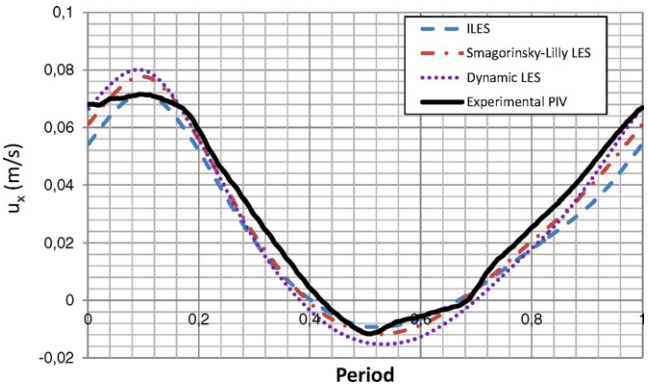

Fig. 9. Experimental and simulated axial velocities through position 2 (see Fig. 7) for the example defined by $Re_o = 646$ ($St = 1.0$, $f = 1$ Hz, $x_0 = 2.65$ mm).

The flow at both conditions is considered chaotic and well outside the range of laminar flow. However, a degree of period repeating occurs within the flow structure at both oscillatory Reynolds numbers. Both flow patterns include eddies of various sizes, with the period repeatability evident in the general formation and propagation of the largest eddies, resulting in a distinct bulk-to-wall mass transfer pattern. Despite the doubling of mixing intensity, these general flow patterns are very similar between the two Re_o. The occurrence of the repeating flow structures in these two cases of differing flow velocities means that simulated flow patterns should also exhibit similar features. This is checked experimentally, as plotted in Fig. 6. It shows experimental flow images for both conditions: the first column of images for $Re_o = 646$ and the second column for $Re_o = 1292$. Each image shows the inter-baffle flow at the same phase position for successive oscillation cycles, and each phase corresponds to 1/10th of the represented oscillation cycle. The period repeatability is similar between the two cases as the domain can be divided into 4 quadrants, each containing a primary large vortex approximately centered at the same location.

For both, LES and ILES, a pressure-based solver was used, with a second order discretization for the pressure. The SIMPLE algorithm (see Patankar, 1980) was utilized for the pressure–velocity coupling. Time integration was performed using the Non-Iterative Time-Advancement Scheme (NITA) (Armsfield & Street, 1999).

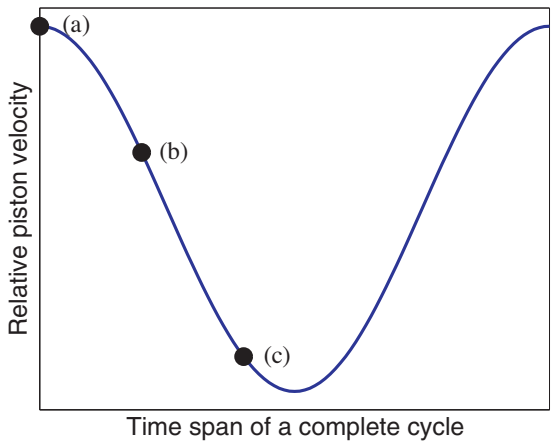

Fig. 10. Phase positions corresponding to photographs and simulation snapshots of the velocity field for the example defined by $Re_o = 646$ ($St = 1.0$, $f = 1$ Hz, $x_0 = 2.65$ mm). The labels (a), (b), and (c) indicate the precise location of those phases in a complete piston oscillation and correspond respectively to times $0/f$, 0.2, and 0.4 of the oscillatory period.

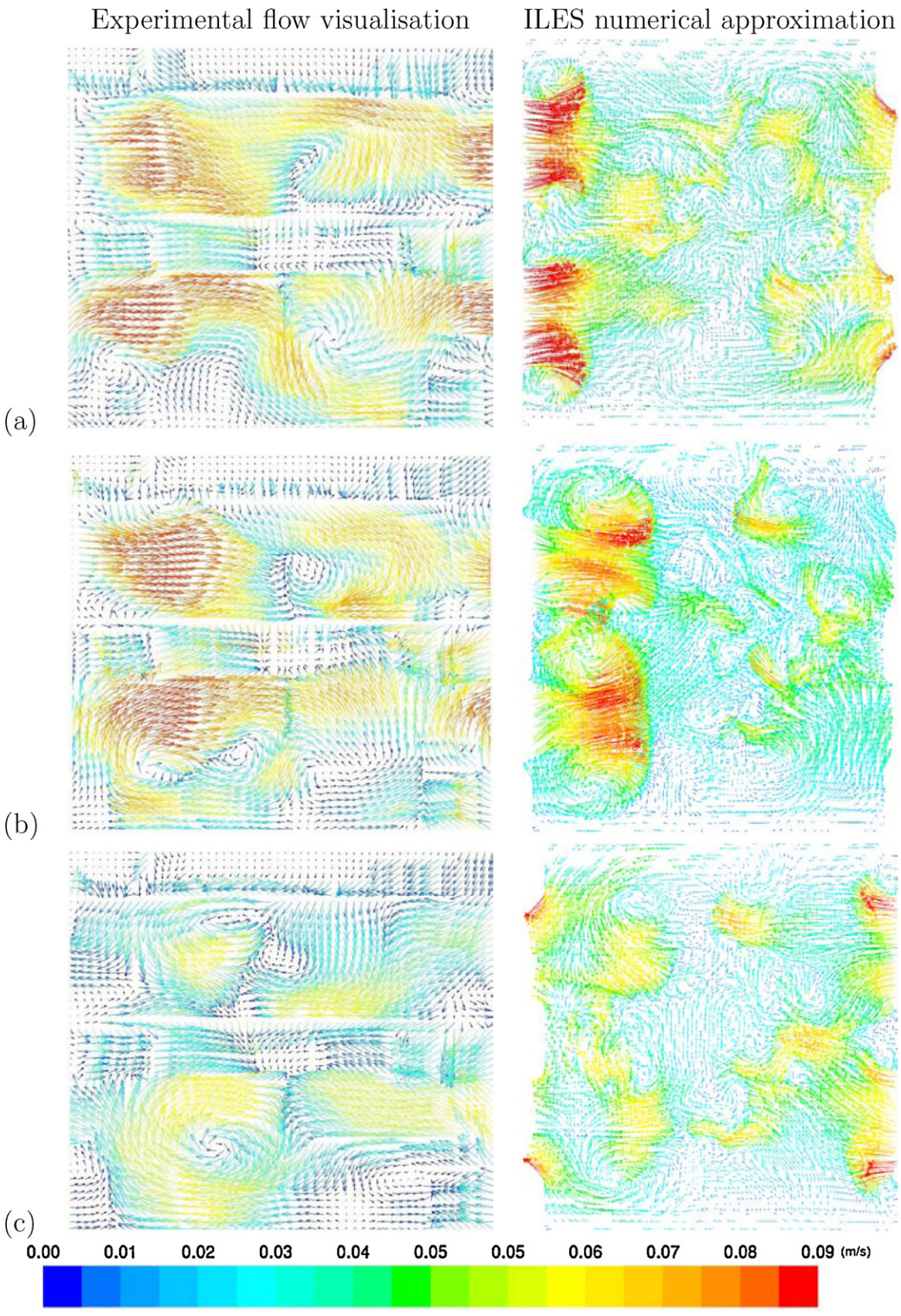

Fig. 11. PIV images of an OBT segment at $Re_o = 646$ ($St = 1.0$, $f = 1$ Hz, $x_0 = 2.65$ mm) showing experimental flow visualization results and numerical approximations using ILES. Labels (a), (b), and (c) refer to Fig. 10, which indicates the phase positions of the images.

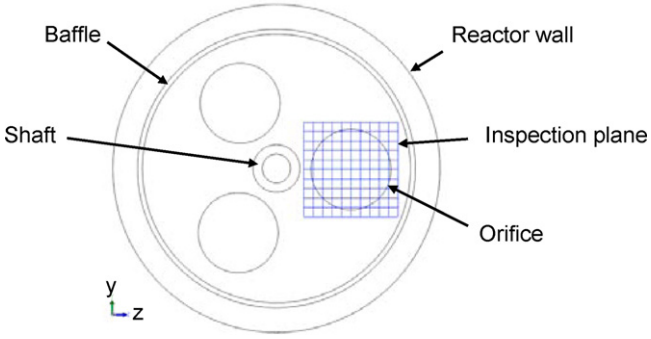

Fig. 12. Schematic view of the LDV inspection plane used for this study.

For the $Re_o = 646$ case, ILES results were compared with experimental results and with an approach using LES with two SGS models: the Dynamic-Smagorinsky model and the Smagorinsky–Lilly model. The latter has been used in the past to simulate oscillatory flow in a single orifice baffled tube with LES (Jian & Ni, 2003; Ni et al., 2003). The Dynamic model is a more complex model that involves an additional filtering. It is less dissipative than the Smagorinsky–Lilly model. In calculations with ILES, gradients were computed using a Least Squares-Based method. This numerical scheme satisfies the fundamental properties outlined in Section 3.2 and thus it is adequate for ILES.

4.1. Analysis of the flow defined by $Re_o = 646$

In this case a time step of $\Delta t = 0.00125$ s was chosen. In order to reduce the influence of the initial conditions, the simulation was run for ten cycles of the piston prior to collection of results.

4.1.1. Phase-averaged local axial and radial velocities

In order to show phase-averaged velocity trends during an oscillation cycle, Fig. 7 shows the velocities of four selected regions (located at the interrogation plane of Fig. 3(b)), phase-averaged across 10 piston oscillation cycles ($Re_o = 646$, $St = 1.0$, $f = 1$ Hz, $x_0 = 2.65$ mm). Velocity magnitudes were examined for all regions within the tube segment. The regions presented in Fig. 7 were identified as having the greatest velocity magnitudes within the OBT segment, and the velocities of those regions were plotted

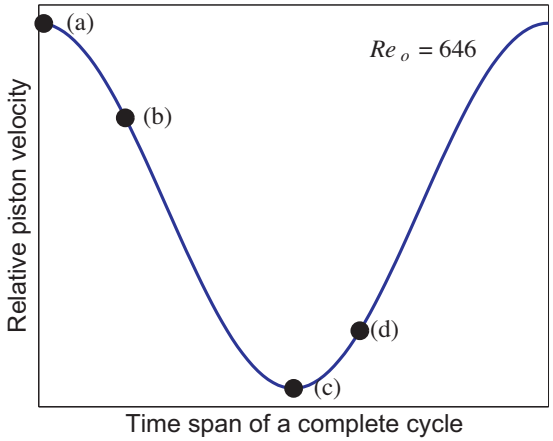

Fig. 14. Phase positions corresponding to simulation snapshots of the vorticity field for the example defined by $Re_o = 646$.

in colors corresponding to the appropriate areas on the included photograph. Each interrogation area is a [7 mm × 7 mm] square.

Fig. 7 shows that, while the axial velocities (u_x) each roughly followed the sinusoidal piston oscillation, the magnitudes differed according to their locations within the OBT. It can also be seen that the u_x in the selected regions near the bottom orifices were greater in magnitude than those directly above them. The u_x magnitudes within all four selected regions were greater when the fluid exited the orifice than when it entered. This difference was due to the change of direction from axial to radial as the fluid passed through the sampled region.

Because the flow is non-uniform, even a small change in selected location could lead to relatively large variance in results. For this reason, careful attention was given to the precision of inspection area location for measurements in the experiments (Fig. 7) and numerical simulations (Fig. 8). The experimentally determined radial velocity (u_y), shown in Fig. 7, is less reliable for measuring the energy transfer in a two-dimensional plane of a three-dimensional OBT, as the radial flow could only be observed and measured in the y direction. However, in combination with axial velocities the u_y peaks are useful for observing periodicity in the radial direction as well as in demonstrating that the radial velocity magnitudes from OFM are of the same order of magnitude as the axial velocity within

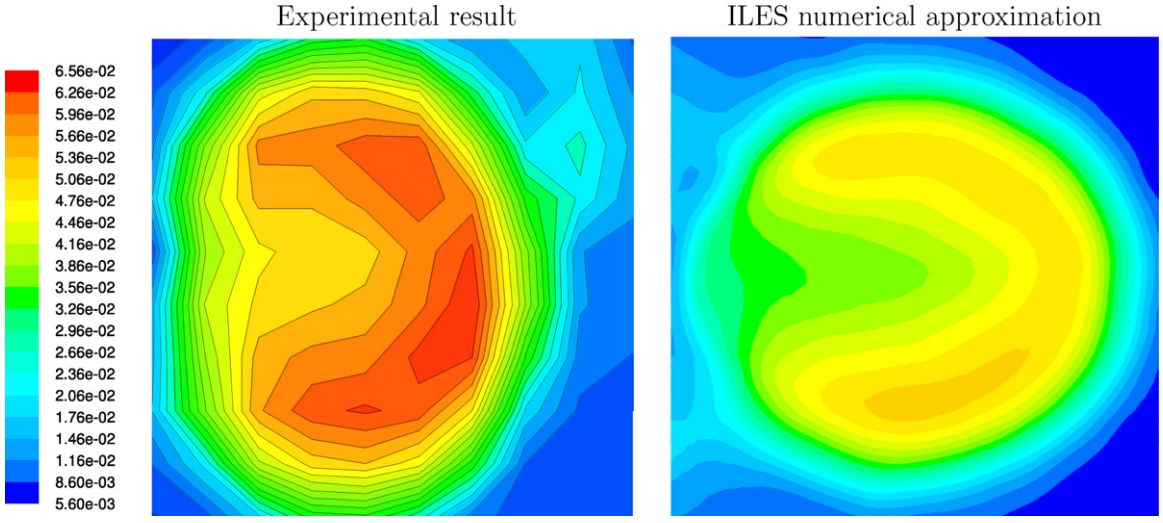

Fig. 13. 2-D LDV (left) and ILES (right) plot of the root mean square of the axial component of the flow velocity (m/s) through an orifice in the OBT during piston oscillations ($Re_o = 646$, $St = 1.0$, $f = 1$ Hz, $x_0 = 2.65$ mm).

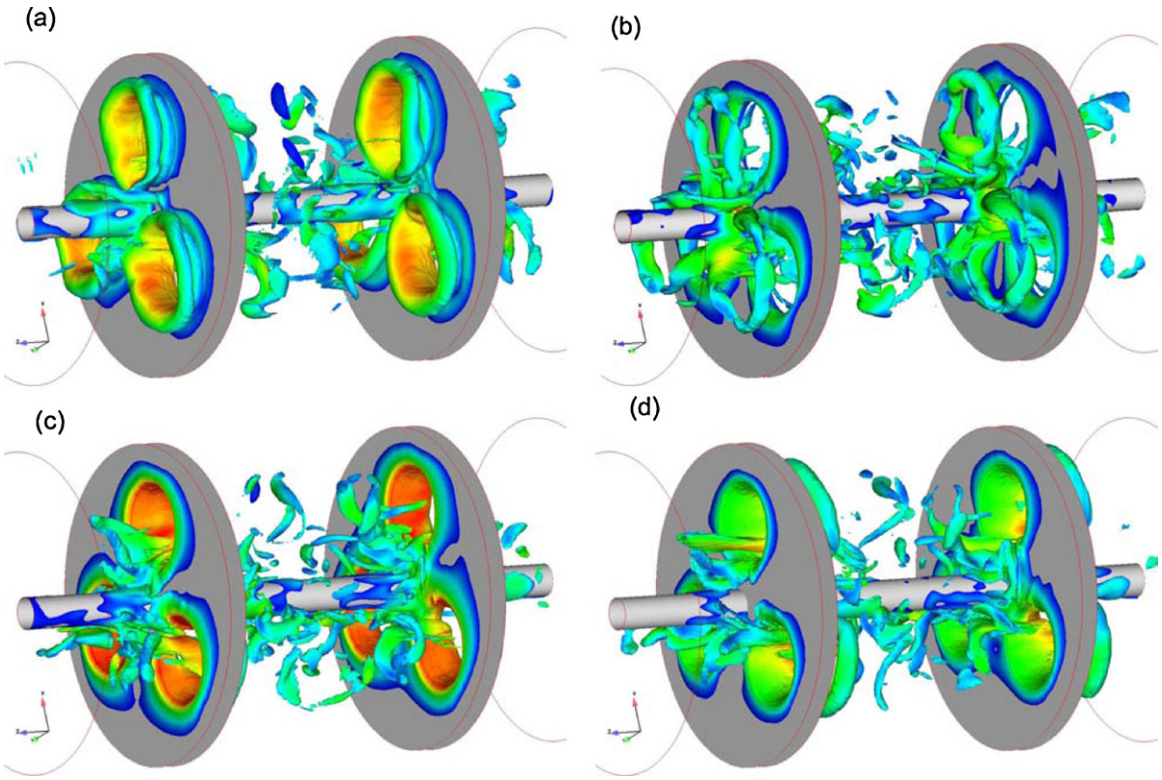

Fig. 15. Detail of the evolution of vortex rings to worm structures for $Re_o = 646$. Vorticity contours of 42 s^{-1} are plotted.

the selected zones. Furthermore, we define a well-mixed zone as one having fluid velocity magnitudes (u_x and u_y) of similar orders of magnitude (one for the axial and two for the radial) to that of the applied piston velocity magnitude. The zones presented in Fig. 7 are for these purposes then classified as well-mixed.

In Fig. 8 we show the axial and radial velocities computed using ILES and LES (with Smagorinsky–Lilly and Dynamic-Smagorinsky subgrid models). By comparing the experimental values in Fig. 7 with the results of the three numerical techniques in Fig. 8, it can be observed that the main patterns of the flow are correctly represented by simulations. Fig. 9 shows the experimental and simulated axial velocities through position 2 (see Fig. 7 for the physical location of position 2). Predictive capabilities of the simulations are compared for the axial velocity profiles, and it can be seen that all three numerical approaches achieve a high degree of precision for this position under these mixing conditions. The figure also shows that ILES matches the experimental peak axial flow velocity more accurately than the other modeling techniques.

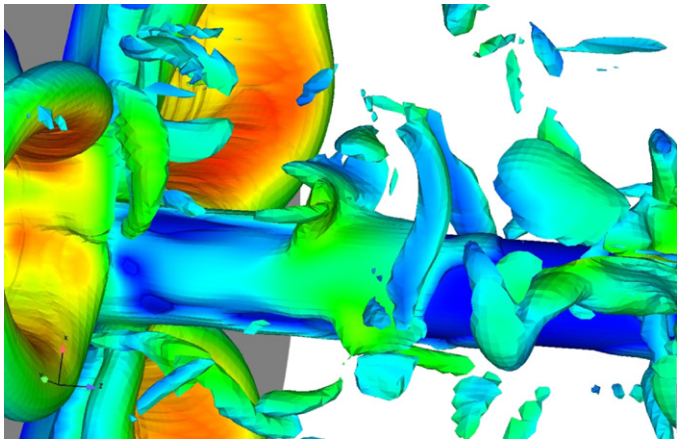

Fig. 16. Detail of vorticity injection at the shaft. The calculation was performed using ILES.

Each numerical approach predicted magnitudes of the axial and radial velocities in the same range of values as the experiments. The simulations also reproduce the phenomenon of reduced axial velocities when the fluid exits the orifice compared with the axial velocities of the fluid when it enters. In addition, the u_y for the selected regions shown in Figs. 7 and 8 are accordingly out of phase with the piston, although the degree of phase off set is not identical to that shown in the experimental flow.

The experimental values in Fig. 7 show that the peak axial velocity through position 1 (0.058 m/s) was approximately 80% of the peak axial velocity through position 2 (0.072 m/s). In contrast, the simulations shown in Fig. 8 each predicted different peak axial values between these two regions, with position 1 consistently presenting peak axial velocities greater than those in position 2. The ILES results predicted a peak axial velocity through position 1 (0.079 m/s) that was 111% of the velocity through position 2 (0.071 m/s). The Smagorinsky–Lilly LES approach predicted a peak axial velocity through position 1 (0.079 m/s) that was 103% of the velocity through position 2 (0.077 m/s), and the Dynamic-Smagorinsky LES predicted a peak axial velocity through position 1 (0.082 m/s) that was 103% of the velocity through position 2 (0.080 m/s). Another discrepancy can be seen in the radial velocity in positions 1–4 of the figures. In those areas, radial velocity never changes sign in the experiments, but it does in the simulations.

Both LES and ILES simulations obtain very similar results. However, ILES seems to be more accurate than LES in the central part of the cycle. Thus, from 0.2 to 0.7 of the oscillatory period axial velocities obtained with ILES present the same patterns as experiments. On the other hand Dynamic-Smagorinsky LES is more accurate in the beginning and in the end of the cycle, but not in the central

part. With Smagorinsky–Lilly LES, axial velocities in positions 1 and 2 and in positions 3 and 4 are almost identical, suggesting a more dissipative behavior of this LES model.

4.1.2. Instantaneous velocity fields

Velocity fields were determined from the simulation taken along the plane defined in Fig. 3(b). Three representative phase positions were selected during an oscillation of the piston. Those phases are shown in Fig. 10, where the dots labeled with the letters (a), (b), and (c) correspond respectively to times 0, 0.2, and 0.4 of the oscillatory period.

Fig. 11 presents experimental and simulated images of the flow segment at $Re_o = 646$ ($St = 1.0$, $f = 1$ Hz, $x_0 = 2.65$ mm). The interrogation plane is the one defined in Fig. 3b. The first column shows experimental PIV pictures of the flow obtained with the procedure outlined in Section 2. The second column shows numerical approximations of the velocity field using ILES. The figure shows that numerical simulation is able to produce results that qualitatively match the experimental results. Thus, values of velocity field and position of vortices are in good agreement with experimental results. Note that any small difference in the initial conditions or in the instant of time where the measurement is made, may lead to very different results.

4.1.3. Analysis of the flow near the baffles

Laser Doppler Velocimetry (LDV) was also used to quantify the mixing in the OBT. Moreover, it was a useful technique for investigating the flow near the central shaft. LDV provides point-wise, time-dependent data, which were used to compare the velocities through different orifices and at different oscillatory conditions. The LDV results were consistent with data gathered during PIV.

LDV measurements taken in the inspection plane located 2 mm from the baffle showed that the shaft had an impact on the flow pattern formation. The interrogation plane is shown in Fig. 12. The measurements show that the close proximity of the shaft to the orifice caused the flow cross-section to be oval-shaped rather than circular.

The geometry of the OBT affects the flow velocity in such a way that the cross-sectional contour lines across the orifice were comprised of c-shaped, higher velocity regions rather than concentric circles, as it is shown in Fig. 13. The irregularity of the velocity contour propagated to an even greater asymmetry further from the orifice. Eventually, at a distance from the baffle, no axial velocity symmetry could be observed across the grid using LDV. This pattern was shown for every set of oscillatory conditions tested.

ILES simulation obtains accurate predictions of the flow in this interrogation area. The simulation partially recovers the experimental oval shape. The side facing the shaft is deviated from the circular shape, but the rest of the flow maintains the circular shape. The c-shape higher velocity regions are well represented by the simulations. The RMS values of the velocity are in agreement with the experiments, although ILES obtains slightly lower values.

4.1.4. Vorticity and vortex dynamics

As it was shown in previous sections, the main patterns of the flow are determined by the periodicity of the piston inlet. It is observed that the flow enters the chamber through inlet holes forming vorticity rings. These structures lead the main behavior of the flow. As the flow develops, these primary vortices break up and they leave the chamber forming worm structures. Four representative phase positions were selected during an oscillation of the piston. They are shown in Fig. 14.

The vortex breaking process is represented in Fig. 15. In this figure, (a) shows the formation of the vortex rings extending from the orifices as the fluid flows through the segment from right to left, (b) shows the completion of the vortex ring formation and separation from the baffle orifices as the applied fluid velocity is null (corresponding to redirection of the piston oscillation), (c) shows the breakup of the rings and the beginning of reorientation of the vortical structures into worms as they are drawn into the orifices as the fluid flow direction has changed, (d) shows the resulting worms passing through the orifice in nearly axial alignment.

Also visible in the vorticity images are worms and other vortical structures, likely from previous oscillation cycles or from vorticity shedding off the central shaft. It is observed that the shaft plays a role in the creation of some of the important structures of the flow. In Fig. 16 it is shown that a vorticity injection originated at the shaft. These bursts of vorticity contribute to increased complexity of the flow, and to some differences in flow patterns between successive cycles.

4.2. Analysis of the flow defined by $Re_o = 1292$

In the case of the $Re_o = 1292$ example, since the frequency of oscillation was larger, a smaller time step was chosen ($\Delta t = 0.000625$ s). Other variables for the numerical methods were the same as in the previous case, and the simulation was run for several piston cycles before the results were collected. Instantaneous velocity fields are presented for the plane defined in Fig. 3. The same representative phase positions as in previous case are presented in Fig. 10, where the dots labeled with the letters (a), (b), and (c) correspond respectively to times 0, 0.2, and 0.4 of the oscillation period.

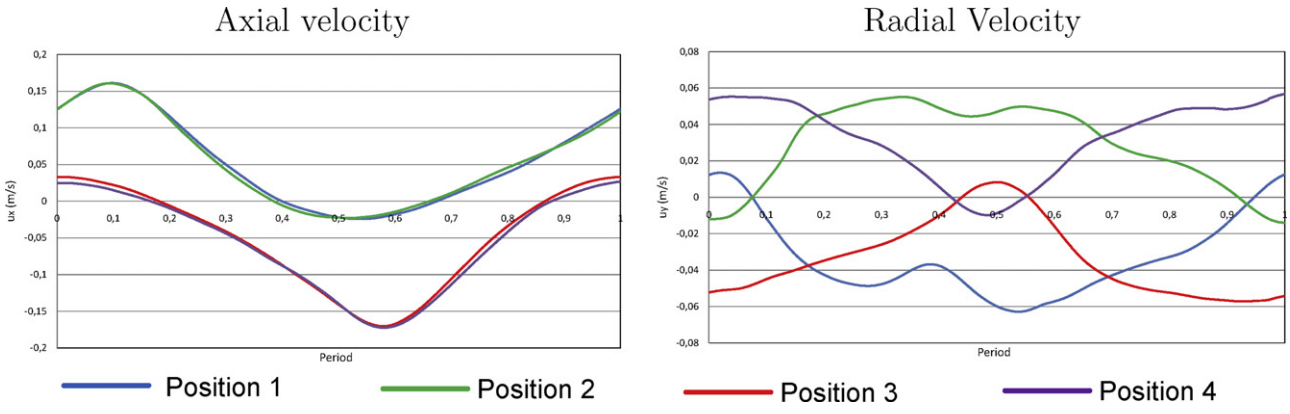

Fig. 17. Numerical results of the phase-averaged local axial and radial velocities of selected regions within the OBT during piston oscillation ($Re_o = 1292$, $St = 1.0$, $f = 2$ Hz, $x_0 = 2.65$ mm). ILES results.

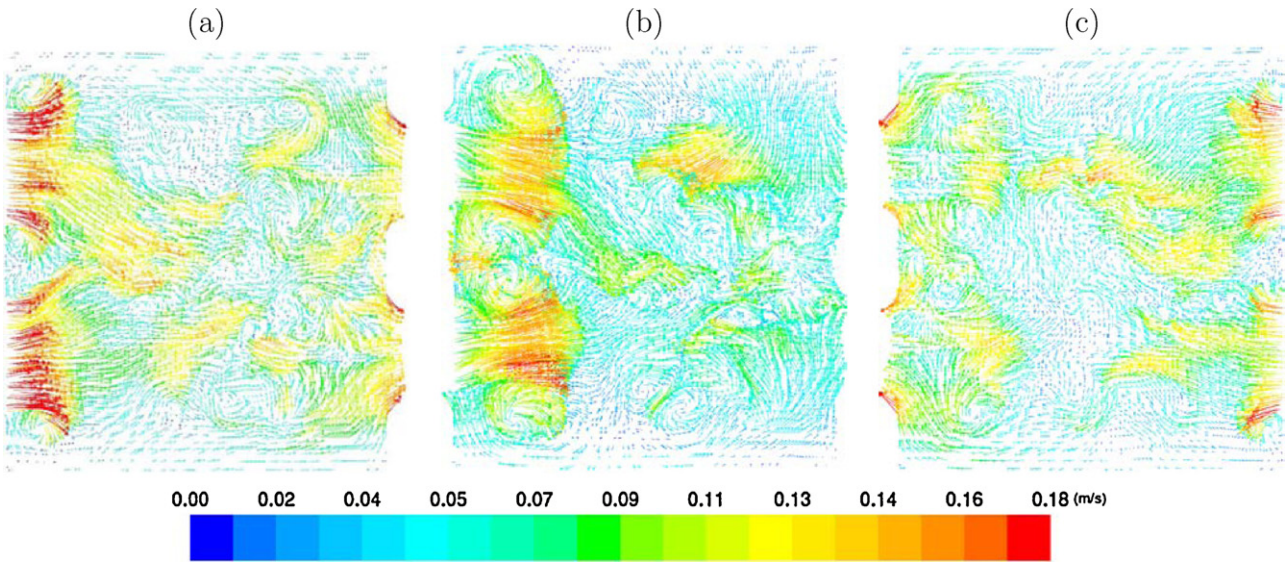

Fig. 18. Numerical approximations of velocity field in an OBT segment at $Re_o = 1292$ ($St = 1.0$, $f = 2$ Hz, $x_0 = 2.65$ mm) using ILES. Labels (a), (b), and (c) refer to Fig. 10, which indicates the phase positions of the images.

4.2.1. Phase-averaged local axial and radial velocities

Fig. 17 shows the axial and radial velocities computed using ILES. It can be seen that the main patterns of these curves are almost identical to those of the $Re_o = 646$. We also observe that the variation of the magnitude of both radial and axial velocities is almost linear with the frequency. The linear relationship of radial and axial velocities with the frequency, indicates that vortex rings formed when the flow enters the chamber determine the flow features in these interrogation areas. In addition, the radial velocity presents the same difference in phase with the piston as in the previous case. From the radial velocity curve, it can be concluded that the mixing is improved when the oscillation frequency is increased.

4.2.2. Instantaneous velocity fields

In Fig. 18 we present the simulation results for the instantaneous velocity fields. The interrogation plane is the same as in the previous case. We observe that the patterns are similar to those for the $Re_o = 646$ case, and the velocity is accordingly increased.

4.2.3. Axial and radial velocities revisited

In this section axial and radial velocities obtained with ILES are compared in the central part of the interrogation plane, as shown in Fig. 19.

The axial velocities are similar in magnitude to those expected (i.e. as the intensity of mixing input has doubled, u_x is

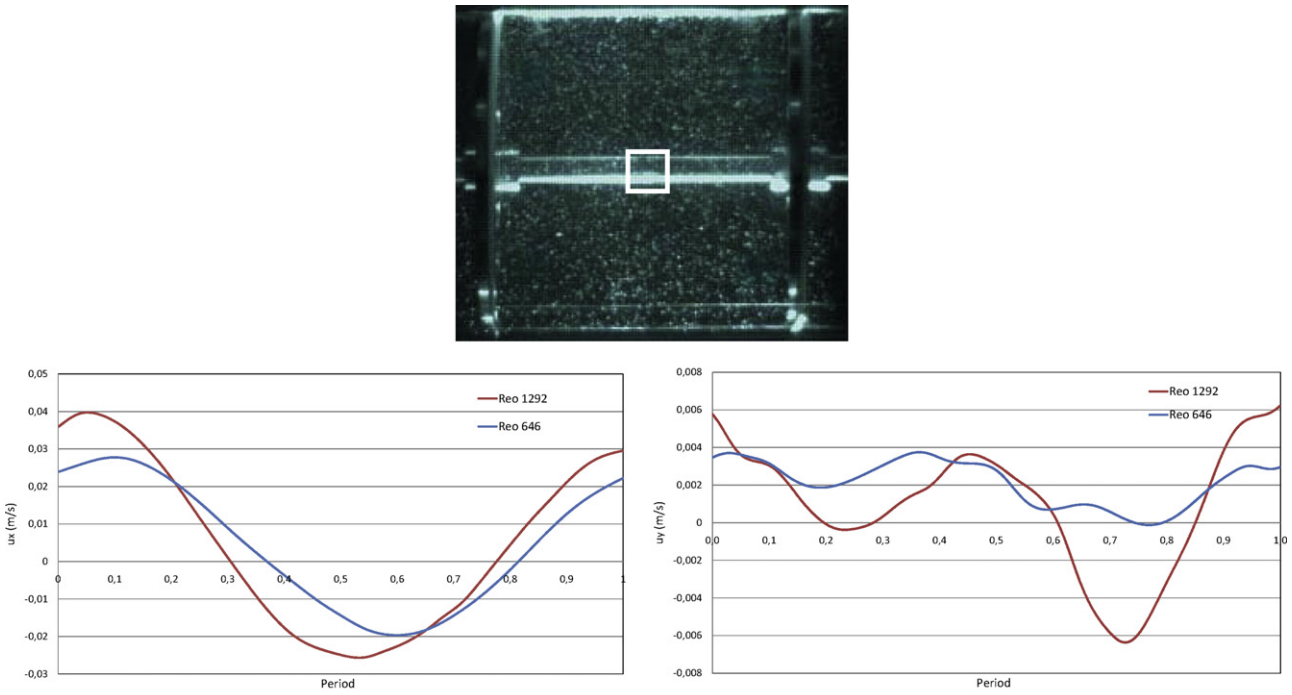

Fig. 19. ILES results of phase-averaged local axial (u_x) and radial (u_y) velocities at the central part of the interrogation plane (white square on the top) within the OBT during piston oscillation for $Re_o = 646$ and $Re_o = 1292$.

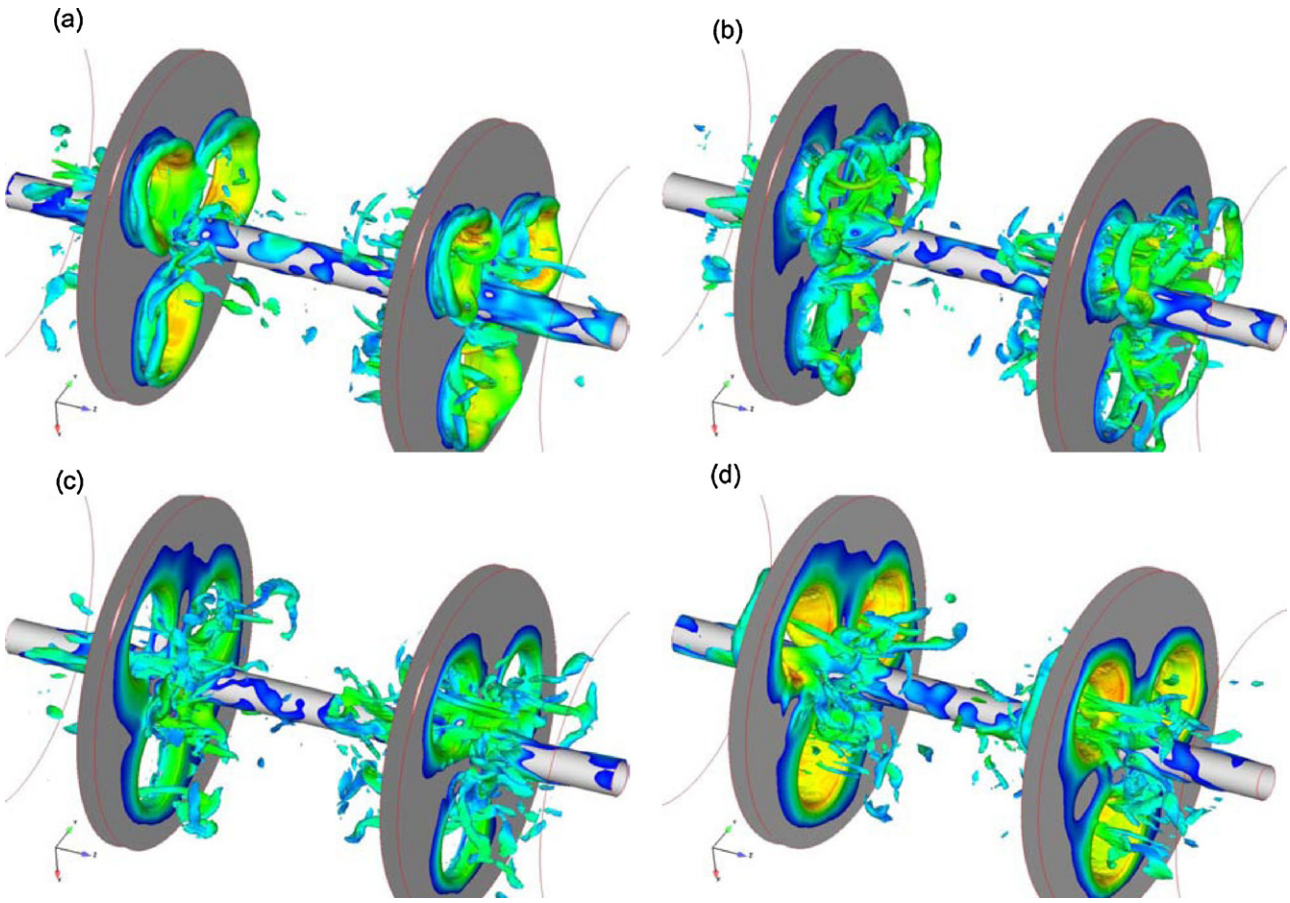

Fig. 20. Detail of the evolution of vortex rings to worm structures for Re_o = 1292. Vorticity contours of 115.5 s^{-1} are plotted.

approximately 1.4 times greater peak to peak). However, the fluctuations in the radial velocities are greater for higher Re_o (i.e. double input intensity results in 3.3 times the peak to peak velocity at this position in the OBT).

These results suggest that the dynamics of the flow in this part of the OBT are very different from dynamics at positions measured in previous sections (see Fig. 7). At those positions the dynamics are meanly determined by the large vortices originated by the flow entering the chamber. At the center of the tube segment, as in Fig. 19, the flow is governed by the interaction of different vortices, and the dynamics are more complicated. However, the periodicity patterns are still observed, as a consequence of the strong periodic character of this flow.

As with the other zones presented in Fig. 7, this central region within the reactor segment can be classified as well-mixed due to its periodicity and because its axial velocity magnitudes are within one order of magnitude and radial velocities within two orders of magnitude of the applied piston velocities. This supports the claims made by others that OFM offers good mixing throughout a tubular reactor or column (for example Fitch et al., 2005; Harvey et al., 2001; Jian & Ni, 2003; Mackley et al., 1993).

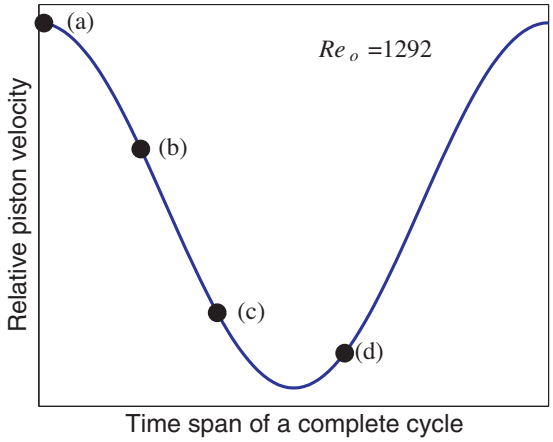

Fig. 21. Phase positions corresponding to simulation 3D snapshots of the vorticity field for the example defined by Re_o = 1292.

4.2.4. Vorticity and vortex dynamics

Fig. 20 shows the breaking-up of the vortices and the conversion into worm structures for this Re_o regime during the phase positions shown in Fig. 21. The main dynamics of the flow are similar to those of the previous case.

Fig. 22 shows the vorticity contours at different planes of the OBT, corresponding to the central part of the cycle (t = 0.5 s) for the two Re_o considered in this work. In the figure, Plane 1 is the interrogation plane of Fig. 3b. Plane 2 crosses the central part of the shaft and is parallel to Plane 1. Plane 3 is symmetric to Plane 1, about the central vertical axial plane of the OBT. Planes 4–6 are parallel to the baffles. Plane 4 is located 2 mm from the exit baffle. Plane 5 is at the center of the OBT, and Plane 6 is located 2 mm from the baffle where the flow enters the OBT segment.

An increase in the vorticity level with Re_o is observed; however, the main patterns of the flow are similar for the two regimes. All of the axial planes present a similar level of vorticity. However, Plane 5 (parallel to the baffles) presents a lower level of vorticity than Planes 4 and 6. This is true for the two regimes studied, and

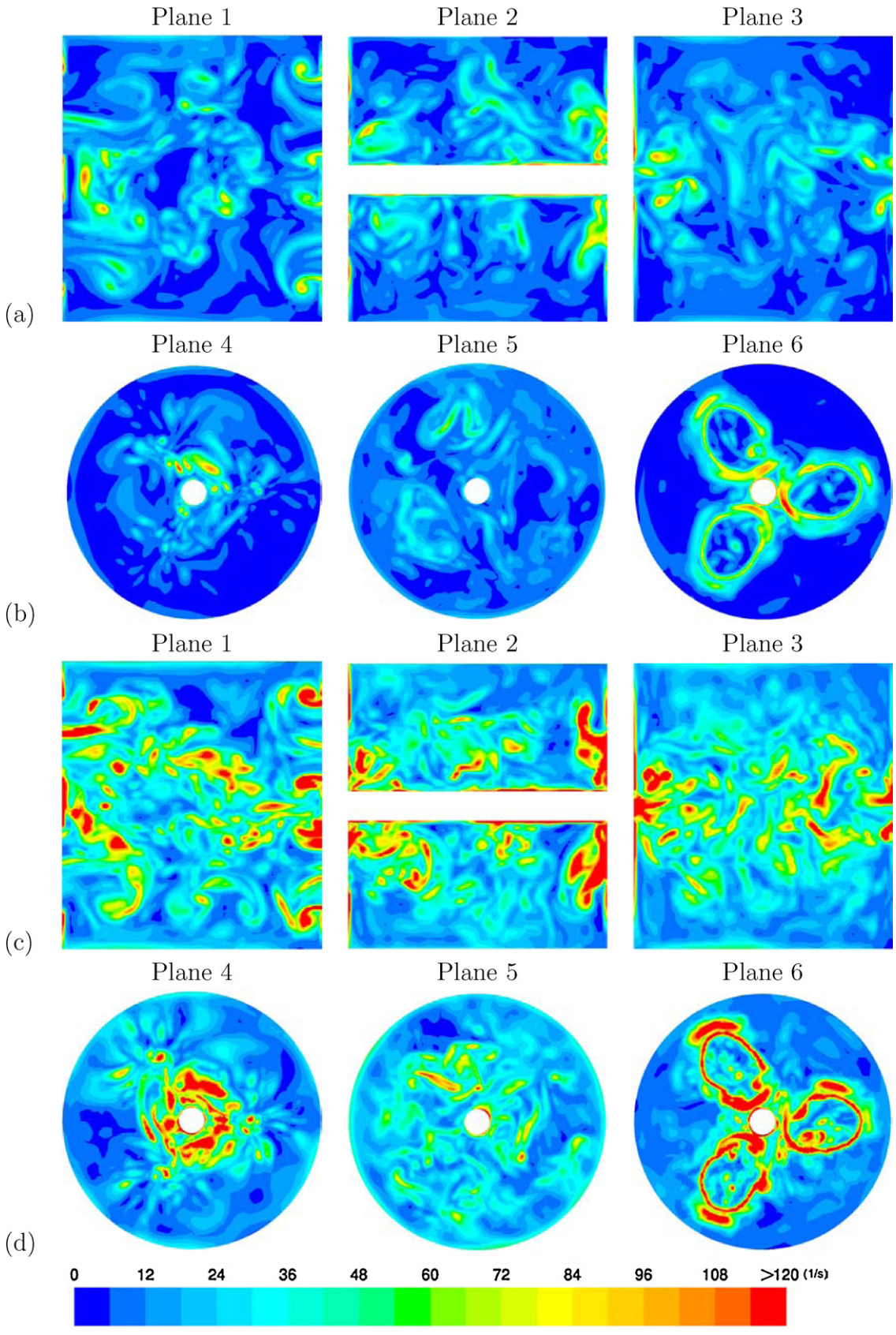

Fig. 22. Vorticity contours for $Re_0 = 646$ (a and b) and $Re_0 = 1292$ (c and d).

accordingly, the high Re_o presents higher vorticity level, and the "worm" structures leaving the domain can be clearly seen. These structures, with high level of vorticity, leave the domain as they are convected by the axial flow. Fig. 22 also shows the important role of the shaft in the increasing of the complexity if the flow. It is an important source of vorticity, which is injected in the main flow.

5. Conclusions

In this work we have presented the application of an Implicit Large Eddy Simulation (ILES) method for the simulation of the flow dynamics of oscillatory flow within a tri-orifice baffled tube (OBT). ILES methodology computes a turbulent flow by solving the Navier–Stokes equations without the addition of turbulent viscosity. This fact makes ILES methodology simpler than conventional LES methods, since when ILES is used, there is no need of any *ad hoc* parameter as required by conventional SGS models. Moreover, the results of the simulations converge to those of Direct Numerical Simulation as the grid is refined. This is an important issue that is not always verified by "eddy-viscosity" approaches.

Results of the ILES simulation for a $Re_o = 646$ flow have been compared with the results obtained using the Smagorinsky–Lilly and the Dynamic Smagorinsky subgrid scale models and with experimentally determined flow patterns and axial and radial velocities in several positions of the OBT. It has been shown in the literature that oscillatory flow mixing (OFM) in the presence of periodically spaced constrictions offers improvement upon both steady flow and oscillatory flow without periodic constrictions (Harvey et al., 2001; Mackley & Ni, 1991), and the advantage to this mixing technique is due to the bidirectional formation and propagation of eddies. Using flow visualisation and particle image velocimetry, our experimental investigation confirmed this effective fluid mixing behaviour. Simulation predictions of different phase positions within the oscillation cycle were compared with matching experimental conditions. Spatial and temporal analyses of velocity vector components indicated that the ILES approach is able to simulate the asymmetric flow patterns of the OBT at least as accurately as the Dynamic-Smagorinsky Large Eddy Simulation, and better than Smagorinsky–Lilly approach. As further validation, ILES of the flow near the baffles was computed and compared with experimental Laser Doppler Velocimetry measurements, showing good agreement of velocity magnitudes and similar responses in the flow near the OBT's central shaft.

Moreover, ILES methodology was used to study the changes in the flow when the Re_o was doubled by doubling the frequency of oscillation. Numerical results showed a linear relationship between oscillation frequency and axial and radial velocities in the interrogation areas near the baffles.

Although numerical investigation further from the baffles demonstrated a more chaotic flow, some semblance of periodicity was observed, with axial and radial velocity magnitudes suggesting mixing within the bulk of the OBT.

Both experimental results and simulation show the effectiveness of the flow geometry used to produce complex eddy motion at modest oscillatory Reynolds numbers where the global mixing appears essentially uniform throughout the domain. Furthermore, it has been shown that ILES is a suitable technique for simulation of oscillatory flow mixing inside an OBT.

Acknowledgments

This work has been partially supported by the *Ministerio de Ciencia e Innovación* (grant #DPI2009-14546-C02-01 and #DPI2010-16496), by R&D projects of the *Xunta de Galicia* (grants #CN2011/002, #PGDIT09MDS00718PR and #PGDIT09REM005118PR) cofinanced with FEDER funds, and the *Universidade da Coruña*.

References

ANSYS. (2009). *FLUENT 12.0 user's guide*.
Armsfield, S., & Street, R. (1999). The fractional-step method for the Navier–Stokes equations on staggered grids: Accuracy of three variations. *Journal of Computational Physics*, *153*, 660–665.
Bazilevs, Y., Calo, V., Cottrell, J., Hughes, T., Reali, A., & Scovazzi, G. (2007). Variational multiscale residual-based turbulence modeling for large eddy simulation of incompressible flows. *Computer Methods in Applied Mechanics and Engineering*, *197*, 173–201.
Beaudan, P., & Moin, P. (1994). Numerical experiments on the flow past a circular cylinder at sub-critical Reynolds numbers. Technical Report. Dept. of Mechanical Engineering, Rept. TF-62, Stanford University.
Boris, J. P., Grinstein, F. F., Oran, E. S., & Kolbe, R. J. (1992). New insights into large eddy simulation. *Fluid Dynamics Research*, *10*, 199–228.
Codina, R., Principe, J., Guasch, O., & Badia, S. (2007). Time dependent subscales in the stabilized finite element approximation of incompressible flow problems. *Computer Methods in Applied Mechanics and Engineering*, *196*, 2413–2430.
Coroneo, M., Montante, G., Paglianti, A., & Magelli, F. (2011). CFD prediction of fluid flow and mixing in stirred tanks: Numerical issues about RANS simulations. *Computers and Chemical Engineering*, *35*, 1959–1968.
Davidson, L. (2010). How to estimate the resolution of an LES of recirculating flow. In M. V. Salvetti, B. Geurts, J. Meyers, & P. Sagaut (Eds.), *Ercoftac Series Quality and reliability of large-eddy simulations II*, *16*, (pp. 269–286). Springer.
Fitch, A., Jian, H., & Ni, X. (2005). An investigation of the effect of viscosity on mixing in an oscillatory baffled column using digital particle image velocimetry and computational fluid dynamics simulation. *Chemical Engineering Journal*, *112*, 197–210.
Germano, M., Piomelli, U., Moin, P., & Cabot, H. (1991). A dynamic subgrid-scale eddy viscosity model. *Physics of Fluids A*, *3*, 1760–1765.
Grinstein, F. F., & Fureby, C. (2002). Recent progress on miles for high Reynolds number flows. *Journal of Fluids Engineering*, *124*, 848–861.
Harvey, A., Mackley, M. R., & Stonestreet, P. (2001). Mixing and dispersion in a baffled tube for steady laminar and pulsatile flow. *Chemical Engineering Science*, *40*, 5371–5377.
Jaworsky, Z., & Dudczak, J. (1998). CFD modelling of turbulent macromixing in stirred tanks. Effect of the probe size and number of mixing indices. *Computers and Chemical Engineering*, *22*, 293–298.
Jian, H., & Ni, X. (2003). On modelling turbulent flow in an oscillatory baffled column – RANS model or large-eddy simulation? *Journal of Chemical Technology and Biotechnology*, *78*, 321–325.
Jian, H., & Ni, X. (2005). A numerical study on the scale-up behavior in oscillatory baffled columns. *Transactions of IChemE*, *83*, 1163–1170.
Jiménez, J. (2007). Recent developments on wall-bounded turbulence. *Revista de la Real Academia de Ciencias. Serie A, Matemáticas*, *101*, 187–203.
Kolmogorov, A. N. (1991). The local structure of turbulence in incompressible viscous fluid for very large Reynolds numbers. *Proceedings of the Royal Society of London, Series A: Mathematical and Physical Sciences*, *434*, 1–9 (translated from the original in Russian – 1941).
Lilly, D. (1996). On the application of the eddy viscosity concept in the inertial subrange of turbulence. *NCAR Manuscript, 123*.
Mackley, M. R., & Ni, X. (1991). Mixing and dispersion in a baffled tube for steady laminar and pulsatile flow. *Chemical Engineering Science*, *46*(12), 3139–3151.
Mackley, M. R., Smith, K. B., & Wise, N. P. (1993). The mixing and separation of particle suspensions using oscillatory flow in baffled tubes. *Transactions of IChemE*, *71A*, 649–656.
Margolin, L. G., & Rider, W. J. (2002). A rationale for implicit turbulence modelling. *International Journal for Numerical Methods in Fluids*, *39*, 821–841.
Margolin, L. G., Smolarkiewicz, P. K., & Sorbjan, Z. (1999). Large eddy simulations of convective boundary layers using nonoscillatory differencing. *Physica D*, *133*, 390–397.
Mittal, R., & Moin, P. (1997). Suitability of upwind-biased finite difference schemes for large-eddy simulation of turbulent flows. *AIAA Journal*, *35*(8), 1415–1417.
Ni, X., Jian, H., & Fitch, A. W. (2002). Computational fluid dynamic modelling of flow patterns in an oscillatory baffled column. *Chemical Engineering Science*, *57*, 2849–2862.
Ni, X., Jian, H., & Fitch, A. W. (2003). Evaluation of turbulent integral length scale in an oscillatory baffled column using large eddy simulation and digital particle image velocimetry. *Chemical Engineering Research and Design*, *78*, 321–325.
Nogueira, X., Cueto-Felgueroso, L., Colominas, I., & Gómez, H. (2010). Implicit large eddy simulation of non-wall-bounded turbulent flows based on the multiscale properties of a high-order finite volume method. *Computer Methods in Applied Mechanics and Engineering*, *199*(9–12), 615–624.
Nogueira, X., Cueto-Felgueroso, L., Colominas, I., & Khelladi, S. (2010). On the simulation of wave propagation with a higher-order finite volume scheme based on reproducing kernel methods. *Computer Methods in Applied Mechanics and Engineering*, *199*, 1471–1490.
Oran, E. S., & Boris, J. P. (1993). Computing turbulent shear flows – A convenient conspiracy. *Computers in Physics*, *10*, 199–228.

Palma, M., & Giudici, R. (2003). Analysis of axial dispersion in an oscillatory-flow continuous reactor. *Chemical Engineering Journal*, *94*, 189–198.
Patankar, S. V. (1980). *Numerical heat transfer and fluid flow*. Taylor and Francis.
Pope, S. B. (2000). *Turbulent flows*. Cambridge: Cambridge University Press.
Porter, D. H., Pouquet, A., & Woodward, P. R. (1992). A numerical study of supersonic turbulence. *Theoretical and Computational Fluid Dynamics*, *4*, 13–49.
Porter, D. H., Pouquet, A., & Woodward, P. R. (1994). Kolmogorov-like spectra in decaying three-dimensional supersonic flows. *Physics of Fluids*, *6*, 2133–2142.
Smagorinsky, J. (1963). General circulation experiments with the primitive equations. I. The basic experiment. *Monthly Weather Review*, *91*, 99–164.
Smith, K. B. (1999). The scale-up of oscillatory flow mixing. Ph.D. thesis. University of Cambridge.
Smith, K., & Mackley, M. R. (2001). An experimental investigation into the scale-up of oscillatory flow mixing in baffled tubes. *Chemical Engineering Science*, *40*, 5371–5377.
Wilcox, D. C. (1994). *Turbulence modelling for CFD*. DCW Industries.